Energy Engineering

Tech Science Press

Doi:10.32604/ee.2025.072997

ARTICLE

Adaptive Droop Control Method for Grid-Forming Low-Voltage Interconnected Converters Considering High-Penetration Distributed Photovoltaics

Shu Zhou, Wenfeng Yang, Guoxing Wu*, Xinming Jiang and Qingmiao Guo

Shenzhen Power Supply Bureau Co., Ltd., Power Grid Planning Research Center, Shenzhen, 518001, China

*Corresponding Author: Guoxing Wu. Email: guoxingwu2025@163.com

Received: 08 September 2025; Accepted: 24 November 2025; Published: 27 April 2026

ABSTRACT: The integration of high-penetration distributed photovoltaic (PV) systems in low-voltage (LV) distribution networks introduces significant challenges, including voltage violations, power quality degradation, and coordination difficulties among multiple distributed energy resources. Grid-forming converters with droop control offer autonomous voltage and frequency regulation capabilities, yet conventional fixed-parameter droop strategies perform poorly in resistance-dominant LV networks under variable PV generation conditions. This paper proposes an adaptive droop control method that dynamically adjusts control parameters to address these challenges. The proposed strategy incorporates three key innovations: (1) power-flow-aware adaptive voltage droop coefficients specifically designed for resistance-dominant networks, (2) a distributed consensus-based optimization algorithm enabling decentralized coordination without centralized infrastructure, and (3) comprehensive stability constraints ensuring robust operation under time-varying parameters. Each grid-forming converter autonomously updates its droop coefficients based on local measurements of PV penetration, voltage deviations, and power flow patterns, while exchanging limited information with neighboring converters to achieve system-wide optimization. The adaptation mechanism includes rate limiters and dead-band functions to prevent parameter chattering and ensure smooth transitions during varying operating conditions. Small-signal stability analysis establishes explicit constraints on the adaptation rates and parameter ranges to maintain adequate stability margins throughout the operating envelope. Simulation validation encompasses three representative scenarios: 24-h steady-state operation with varying PV penetration (30%–120%), severe cloud transients with 70% generation drops, and evening load pickup transitions. Results demonstrate superior performance with voltage regulation within 0.95–1.05 p.u. at 120% PV penetration, power sharing errors below 3% vs. 15% for conventional control, and 65% faster transient response (0.8 vs. 2.3 s settling time). Compared to fuzzy logic methods, the proposed approach achieves 55% error reduction while eliminating expert knowledge requirements. The method enables resilient high-penetration PV integration in LV distribution networks through fully decentralized operation.

KEYWORDS: Adaptive droop control; grid-forming converters; distributed photovoltaic systems; low-voltage distribution networks; power sharing optimization

1 Introduction

The rapid growth of distributed photovoltaic (PV) systems has changed the operational paradigm of a modern power network fundamentally [1]. By virtue of the gradual growth of the contribution of power sources from renewable energies and that of low-voltage (LV) distribution network solar PV in specific, conventional procedures of operating grids are challenged more than ever before in keeping the network stable and of elevated power quality [2]. The International Energy Agency has reported that in recent years, the world's cumulative capacity of added solar power has risen to record levels, most of it through

distributed PV systems [3]. The movement in the direction of distributed generation requires new control strategies capable of properly managing two-way power transfers and voltage changes that occur with high-penetration PV systems [4]. Grid-forming converters have emerged as a promising solution to address the stability issues brought about by high penetration of renewable energy in distribution networks [5]. Unlike conventional grid-following converters dependent on stiff grid voltages, grid-forming converters can independently establish and regulate bus voltage magnitude and frequency; therefore, they are able to provide services necessary for the grid [6]. At LV interconnected networks with the implementation of grid-forming control, improved robustness is thereby achieved while the simultaneous integration of many different distributed energy resources into one system is made feasible without weakening its stability [7]. Recent studies have also shown that under a wide range of fault conditions, grid-forming converters can greatly improve the dynamic response of distribution networks [8].

According to [9], the basic control principle of parallel converters is power sharing (droop control) in DG (distributed generation) systems. The traditional droop control method makes the converter emulate the behaviors of a synchronous generator. A linear relationship is established, which expresses active power as being directly proportional to frequency and reactive power as being directly proportional to voltage magnitude [10]. The common resistive behavior of LV lines in LV networks is quite unlike the inductive ones of the past and so places new demands on conventional droop control [11,12]. That is, the impedance feature of these needs to be changed to suit the strength of active power and reactive power in an LV distribution network [13]. With the penetration of high-penetration distributed PV systems, the control design pattern of the grid-forming converters becomes complex [14]. Photovoltaic power has inherent randomness and uncertainty. In this type of dynamic operation, conditions under which the conventional constant parameter droop control strategies are incapacitated from functioning well, a different choice is vitally necessary [15]. There exist reverse currents in some areas in state with high PV power generation. It will cause an overvoltage condition in the area, and the abrupt change in the solar radiation may lead to power quality and voltage instability [16]. Apart from that, different PV inverters have different operation behaviors, and the PV inverters are to be synchronized with the grid-forming converter. Either the two supplement each other, or the problem will happen [17].

As a matter of fact, adaptive control strategies, the novel method to gently periphery the fault of conventional droop control for high penetration PV, are receiving increased attention [18]. Adaptive droop control can not only guarantee power sharing accuracy but also provide stable system operation across a wide range of conditions by continuously varying its control parameters based on current environmental conditions [19]. There exist different suggestions for the adaptive mechanisms of the latest studies. They include the utilization of fuzzy logic-based methods [20], model predictive control [21], and even machine learning algorithms to improve how droop-controlled converters perform effectively at lower power levels or under adverse conditions than before [22]. The advanced control methodologies overcome the limitations inherent in large-scale renewable energy generation, changing grid conditions, and so on [23]. The stability analysis of adaptive droop control systems is mainly a problem of how to deal with guaranteeing the reliability of operation [24]. The changing adaptive parameter system may bring in extra dynamics that have an impact on system stability margins without necessarily breaking it down completely [25]. Functional modeling with feedback has become a widely accepted technique for evaluating the stability of droop-controlled converter systems, yielding a knowledge basis surrounding the relationship between control parameters and eigenvalues of system history (or plant dynamics) characteristics, such as participation factors [26]. Incorporation of adaptive mechanisms calls for an expansion of the stability analysis framework, which covers where parameter variation takes place and how the varying parameter interacts with system dynamics [27].

Recent studies have explored various adaptive control strategies to address the limitations of fixed-parameter droop control. Fuzzy logic-based methods [20] can adjust parameters intelligently but require expert knowledge and impose computational burdens. Model predictive control approaches [21] achieve optimal performance but depend heavily on accurate system models that may not be available in real-time. Machine learning algorithms [22] show promise but necessitate extensive training data and offline learning phases. As summarized in Table 1, these methods face practical implementation challenges in terms of computational complexity, model dependency, or data requirements. In contrast, the distributed consensus-based approach proposed in this work enables real-time adaptive parameter adjustment without centralized coordination or prior training.

Table 1: Comparison of adaptive droop control methods

Reference	Method	Limitations
[20]	Fuzzy logic-based control	Requires expert knowledge; computationally complex
[21]	Model predictive control	Dependent on accurate system models
[22]	Machine learning algorithms	Requires extensive training data
This work	Distributed consensus optimization	No centralized coordination; real-time capability

The main contributions of this work compared to existing methods are threefold: (1) adaptive voltage droop coefficients that incorporate power flow direction for resistance-dominant LV networks (Eq. (18)), (2) distributed consensus optimization for decentralized coordination among converters, and (3) stability constraints ensuring robust operation under time-varying adaptive parameters through rate limiters (Eq. (19)) and eigenvalue analysis (Eq. (27)). Existing adaptive methods [20–22] primarily address inductive networks or rely on centralized control, whereas the proposed approach is specifically tailored for resistive LV systems with decentralized implementation.

This paper proposes a novel adaptive droop control method for grid-forming LV interconnected converters that specifically addresses the challenges posed by high-penetration distributed PV systems, building upon previous research while introducing innovative solutions to enhance system performance and stability. The presented method varies the droop coefficients in real-time with the PV penetration level measurements, the status of the grids, and the power flow patterns in order to achieve optimal power sharing and voltage control across the vast range of operation scenarios. Through the application of stringent theoretical derivation and simulation case studies, the paper demonstrates the effectiveness of the proposed adaptive control method in maximizing distributed PV systems penetration with stable system operation in LV distribution networks.

2 System Modeling and Problem Formulation

2.1 LV Interconnection System Topology

The low-voltage interconnection system consists of several distributed photovoltaic units interfaced with the LV distribution network through multiple grid-forming converters, as presented in Fig. 1. The structure is constituted by power conversion units in parallel with LC output filters to suppress switching harmonics and offer distributed voltage support at the local level. Distribution lines with resistance-dominant impedance characterized by R/X values larger than 5 in typical LV networks connect the converters in peer fashion without the necessity for centralized communication. The grid-forming converters autonomously

work in synchronization using the droop control system and form a peer architecture without the necessity of centralized communication. The point of common coupling (PCC) is the connecting juncture between the distributed converter system and the upstream medium-voltage network using a distribution transformer. Local loads are distributed across the network resulting in various power flow scenarios based on PV generation and consumption patterns at the node level. Power sharing between converters is achieved while maintaining the voltage regulation within acceptable ranges using the interconnection topology. During high PV generation periods, excess power flows bidirectionally through the distribution transformer, potentially causing voltage rise issues that must be addressed through appropriate control strategies.

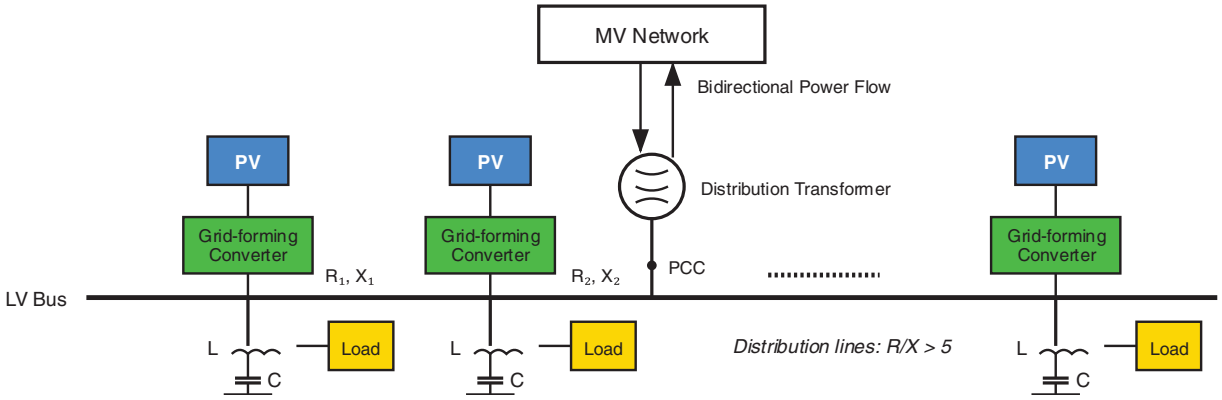

Figure 1: LV interconnection system topology

2.2 Mathematical Model of Grid-Forming Converters

The control strategy presented in this work fundamentally operates in grid-forming mode, where the converter functions as a voltage source that establishes and regulates the voltage magnitude and frequency at its terminal without relying on a pre-existing grid voltage reference. This distinguishes it from grid-following converters, which operate as current sources synchronized to an external voltage established by other grid elements. The grid-forming capability is manifested through the voltage-controlled operation described by Eqs. (1)–(7), where the converter's output voltage serves as the controlled variable rather than the output current. While the droop control mechanism in Eqs. (4) and (5) employs classical droop theory originally developed for synchronous generators, its application here is fundamentally different from grid-following inverters, which rely on phase-locked loops for synchronization and operate as current sources under grid-connected conditions. In the grid-forming paradigm, the droop relationships directly govern the autonomous voltage and frequency formation process, enabling the converter to operate independently or in parallel with other grid-forming units without a stiff grid voltage for synchronization. This voltage-source behavior, combined with the primary frequency support capability provided by the power-frequency droop mechanism, qualifies the proposed converter system as a true grid-forming topology capable of supporting weak grids and islanded operation scenarios commonly encountered in high-penetration PV distribution networks.

The mathematical modeling of grid-forming converters constitutes the foundation for control design and stability analysis in LV interconnected systems. The converter power stage dynamics with LC output filters are represented by well-established differential equations in the synchronous dq reference frame [6,26], from which the instantaneous active and reactive powers are derived to implement droop control for autonomous power sharing among parallel converters.

The droop control mechanism establishes the relationship between the converter's output frequency and voltage magnitude with the measured active and reactive powers. The frequency droop characteristic is expressed as

$$\omega = \omega^* - m_p \left(P - P^*\right) \tag{1}$$

where ω^* represents the nominal angular frequency, m_p is the frequency droop coefficient, and P^* denotes the active power reference. Similarly, the voltage droop relationship is given by

$$V = V^* - n_q \left(Q - Q^*\right) \tag{2}$$

where V^* is the nominal voltage magnitude, n_q represents the voltage droop coefficient, and Q^* is the reactive power setpoint. Although the proposed control strategy employs classical droop theory originally derived from the governor and excitation characteristics of synchronous generators, its implementation fundamentally differs from conventional grid-following applications in terms of operational mode. Classical droop control can be applied in two distinct paradigms: voltage-source mode (grid-forming) and current-source mode (grid-following). In the voltage-source mode adopted in this work, the converter operates as a controllable voltage source where the droop Eqs. (1) and (2) directly synthesize the voltage reference (V^*, ω^*) that the inner control loops impose on the power stage, thereby establishing the grid voltage and frequency autonomously. Conversely, in current-source mode implementations common to grid-following inverters, the same droop equations merely calculate current injection references (I_d^*, I_q^*) or power references that the converter delivers into an already-established grid voltage maintained by other sources. The fundamental distinction lies not in the mathematical form of the droop equations themselves, but in their control objectives: grid-forming mode uses droop to establish the voltage reference, while grid-following mode regulates current injection into an existing grid voltage. Therefore, although this work leverages the well-established principles of droop control theory, its application within a voltage-source architecture qualifies it as a grid-forming solution rather than a grid-following controller.

The droop coefficients must be properly designed to ensure both system stability and desired power sharing among converters.

Eqs. (4) and (5) constitute the fundamental essence of grid-forming operation and distinguish the proposed control architecture from grid-following paradigms. In grid-forming mode, these droop relationships do not merely describe power regulation characteristics—they directly determine the voltage reference magnitude (V^*) and angular frequency (ω^*) that the converter synthesizes autonomously. The converter establishes these electrical quantities based solely on local power measurements (P and Q) without requiring phase-locked loop (PLL) synchronization to an external grid voltage, which is the hallmark of grid-following operation. Specifically, Eq. (1) enables the converter to autonomously adjust its output frequency in response to active power imbalances, thereby providing synthetic inertia analogous to synchronous generators, while Eq. (2) governs autonomous voltage magnitude regulation based on reactive power flow. This self-regulating mechanism allows multiple grid-forming converters to operate in parallel and achieve stable load sharing through the inherent droop characteristics, forming a decentralized voltage and frequency control hierarchy. In contrast, grid-following converters would use PLL to track grid frequency and employ current control loops to inject power according to external references, fundamentally lacking the autonomous voltage-forming capability embodied in Eqs. (1) and (2). Therefore, the mathematical structure of these droop relationships, where frequency and voltage magnitude are dependent variables controlled by power measurements, represents the core enabling feature that qualifies this converter system as grid-forming.

To implement the voltage and current control loops, the converter employs a cascaded control structure with an outer voltage loop and an inner current loop, utilizing standard PI controllers with feed-forward decoupling terms as described in [6,8]. The voltage controller generates current references, which are then tracked by the inner current control loop to determine the converter bridge voltage commands.

The complete state-space representation of the grid-forming converter system can be formulated by combining the power stage dynamics, control loops, and droop characteristics. The state vector is defined as

$$\mathbf{x} = \left[i_{od}, i_{oq}, v_{od}, v_{oq}, \phi_d, \phi_q, \gamma_d, \gamma_q, \delta, P_f, Q_f \right]^T \tag{3}$$

where ϕ_d and ϕ_q are the voltage controller integral states, γ_d and γ_q represent the current controller integral states, δ is the angle deviation, and P_f and Q_f are the filtered power measurements. The linearized state-space model around an operating point can be expressed as

$$\Delta\dot{\mathbf{x}} = \mathbf{A}\Delta\mathbf{x} + \mathbf{B}\Delta\mathbf{u} \tag{4}$$

where $\mathbf{A}$ is the system matrix containing the linearized dynamics, and $\mathbf{B}$ represents the input matrix. This state-space formulation enables eigenvalue analysis and provides insights into the system stability characteristics under various operating conditions and control parameter selections.

The system matrix $\mathbf{A}$ and input matrix $\mathbf{B}$ in Eq. (4) can be derived by linearizing the converter dynamics around the equilibrium point. The system matrix has the following block structure:

$$\mathbf{A} = \begin{bmatrix} \mathbf{A}_{11} & \mathbf{A}_{12} & \mathbf{A}_{13} \\ \mathbf{A}_{21} & \mathbf{A}_{22} & \mathbf{A}_{23} \\ \mathbf{A}_{31} & \mathbf{A}_{32} & \mathbf{A}_{33} \end{bmatrix} \tag{5}$$

where the submatrices correspond to power stage dynamics ($\mathbf{A}_{11}$), controlloopdynamics ($\mathbf{A}_{22}$), and droop-power coupling ($\mathbf{A}_{33}$). The key coupling elements are:

$$\mathbf{A}_{11} = \begin{bmatrix} -R/L & -\omega_0 & -1/L & 0 \\ \omega_0 & -R/L & 0 & -1/L \\ 1/C & 0 & 0 & -\omega_0 \\ 0 & 1/C & \omega_0 & 0 \end{bmatrix}, \quad \mathbf{A}_{22} = \begin{bmatrix} 0 & 0 & -1 & 0 \\ 0 & 0 & 0 & -1 \\ -1 & 0 & 0 & 0 \\ 0 & -1 & 0 & 0 \end{bmatrix} \tag{6}$$

The droop-related submatrix $\mathbf{A}_{33}$ contains the frequency and voltage regulation dynamics:

$$\mathbf{A}_{33} = \begin{bmatrix} 0 & -m_p \cdot \frac{3V_0}{2} & 0 \\ -n_q \cdot \frac{3I_0}{2} & 0 & 0 \\ 0 & 1/\tau_f & -1/\tau_f \end{bmatrix} \tag{7}$$

where τ_f is the power filter time constant, and V_0, I_0 are operating point values. The input matrix is:

$$\mathbf{B} = \left[\mathbf{0}_{4\times2} \ \mathbf{I}_{2\times2} \ \mathbf{0}_{5\times2} \right] \tag{8}$$

where the inputs correspond to reference power commands $\Delta\mathbf{u} = \left[\ \Delta P^*; \Delta Q^* \ \right]^T$.

2.3 Impact Analysis of High PV Penetration

High penetration of distributed photovoltaic systems fundamentally alters the operational characteristics of low-voltage distribution networks, transforming them from passive consumption-oriented systems to active networks with bidirectional power flows. The penetration level can be quantified as

$$\lambda_{PV} = \frac{P_{PV}^{total}}{P_{load}^{peak}} \times 100\% \tag{9}$$

where P_{PV}^{total} represents the total installed PV capacity and P_{load}^{peak} denotes the peak load demand. When penetration levels exceed 50%–60%, significant technical challenges emerge that compromise system stability and power quality.

The most prominent issue is voltage rise during periods of high solar generation and low load consumption. The voltage at any node i along the feeder can be approximated as

$$V_i = V_0 + \sum_{j=1}^{i} \frac{R_j P_j + X_j Q_j}{V_{nom}} \tag{10}$$

where V_0 is the substation voltage, R_j and X_j are the resistance and reactance of line segment j, and P_j and Q_j are the net active and reactive power flows. In LV networks where $R >> X$, active power injection from PV systems directly contributes to voltage rise, potentially exceeding the permissible range of $V_{nom} \pm 10\%$.

Power flow reversal occurs when local PV generation exceeds demand, characterized by

$$P_{reverse} = P_{PV} - P_{load} > 0 \tag{11}$$

This reversal creates operational challenges for protection systems and voltage regulators designed for unidirectional flow. The variability of solar irradiance introduces rapid power fluctuations quantified by the ramp rate

$$\frac{dP_{PV}}{dt} = \eta A \frac{dG}{dt} \tag{12}$$

where η is the conversion efficiency, A is the array area, and G is the solar irradiance. Cloud transients can cause ramp rates exceeding 60% of rated capacity per minute, creating voltage flicker and frequency deviations.

The interaction between multiple PV inverters and grid-forming converters introduces harmonic distortion and resonance risks. The total harmonic distortion increases with penetration level according to

$$THD_v = \sqrt{\sum_{h=2}^{\infty} \left(\frac{V_h}{V_1} \right)^2} \tag{13}$$

where V_h represents the h-th harmonic component. Furthermore, the reduced system inertia due to converter-interfaced generation affects frequency stability, with the rate of change of frequency given by

$$\frac{df}{dt} = \frac{P_{imbalance}}{2H_{sys}S_{base}} \tag{14}$$

where H_{sys} is the equivalent system inertia and S_{base} is the system base power. These multifaceted impacts necessitate advanced control strategies that can adaptively respond to varying PV penetration conditions while maintaining system stability and power quality within acceptable limits.

The above analysis demonstrates that high *PV* penetration causes voltage violations and power fluctuations that cannot be adequately addressed by conventional fixed-parameter droop control. To mitigate these issues, the adaptive droop coefficient design in Eqs. (19)–(21) directly targets the voltage deviations described in Eq. (14) and the power ramp rates characterized in Eq. (16), enabling real-time parameter adjustment based on operating conditions.

3 Adaptive Droop Control Strategy Design

3.1 Limitations of Conventional Droop Control

Conventional droop control schemes, while effective in transmission systems with predominantly inductive impedances, reveal key shortcomings in low-voltage distribution systems with high penetration rates of PVs. Conventional droop coefficients cannot accommodate dynamic operating conditions caused by variable renewable power sources. When applied to resistive-dominant LV networks, the key assumption of decoupled P-f and Q-V relationships no longer holds, and power sharing becomes inaccurate due to cross-coupling effects that degrade system performance. Conventional droop expressions assume constant impedance ratios, which becomes invalid under varying network conditions caused by fluctuating PV output and loading patterns.

The inherent tradeoff between voltage regulation and power sharing precision poses significant challenges in high-penetration applications. Small droop coefficients favor voltage quality but result in unequal power sharing across converters, while larger coefficients improve power sharing but compromise voltage quality. Such a static tradeoff is unable to accommodate the wide range of operation that is often necessary in networks with highly fluctuating PV generation. Moreover, the conventional droop control has a slow dynamic response across fast changes of irradiance because the system is unable to keep up with stability across cloud transients or fast changes in loads. The inability of differentiating between system-level and local disturbances often translates into the unwarranted control actions that result in oscillations and low system damping. These drawbacks give rise to the necessity of developing control methods that adaptively change parameters in accordance with changing system operation in real-time.

3.2 Adaptive Droop Coefficient Design Method

The proposed adaptive droop control strategy dynamically adjusts the droop coefficients based on real-time measurements of *PV* penetration level, voltage deviation, and power flow conditions. The adaptive frequency droop coefficient is designed as

$$m_p^{ada} = m_p^0 \cdot K_p\left(\lambda_{PV}, \Delta V\right) \tag{15}$$

where m_p^0 represents the base droop coefficient and K_p is the adaptive gain function. The gain function is formulated as

$$K_p = \left(1 + \alpha_p \lambda_{PV}\right)\left(1 + \beta_p |\Delta V|\right) \tag{16}$$

where α_p and β_p are tuning parameters, and $\Delta V = V_{measured} - V_{nom}$ represents the voltage deviation from nominal.

For the voltage droop coefficient, the adaptive mechanism incorporates power flow direction and magnitude:

$$n_q^{ada} = n_q^0 \cdot K_q\left(P_{flow}, Q_{flow}\right) \tag{17}$$

where $K_q = \frac{1}{1+\gamma_q|P_{flow}/P_{rated}|} \cdot \left(1 + \delta_q|Q_{flow}/Q_{rated}|\right)$. This formulation ensures tighter voltage regulation during reverse power flow conditions while maintaining reactive power sharing capability. The coefficients γ_q and δ_q are designed using particle swarm optimization to minimize the objective function.

$$J = w_1 \sum_{i=1}^{n} (\Delta V_i)^2 + w_2 \sum_{i=1}^{n} (\Delta P_i)^2 + w_3 \sum_{i=1}^{n} (\Delta Q_i)^2 \tag{18}$$

where w_1, w_2, and w_3 are weighting factors.

To ensure stability during coefficient transitions, a rate limiter is implemented:

$$\frac{dm_p^{ada}}{dt} \leq \rho_m \text{ and } \frac{dn_q^{ada}}{dt} \leq \rho_n, \tag{19}$$

where ρ_m and ρ_n are the maximum allowable rates of change. The adaptive mechanism also incorporates a dead-band function to prevent unnecessary adjustments:

$$m_p^{ada}(k+1) = \begin{cases} m_p^{ada}(k) \cdot K_p(k+1) & \text{if } |K_p(k+1) - K_p(k)| > \epsilon \\ m_p^{ada}(k) & \text{otherwise} \end{cases} \tag{20}$$

where ϵ is the dead-band threshold. This design ensures smooth adaptation while avoiding chattering behavior during steady-state operation.

The adaptive parameters α_1 and α_2 are tuned using particle swarm optimization (PSO) with the objective function defined in Eq. (23). The weighting coefficients are empirically set as $w_1 = 0.5$, $w_2 = 0.3$, and $w_3 = 0.2$ to prioritize voltage quality over power sharing accuracy and transient response, with detailed tuning procedures omitted for brevity.

3.3 Power Sharing Optimization Algorithm

The power sharing optimization algorithm employs a distributed consensus-based approach to achieve accurate power distribution among grid-forming converters while maintaining voltage regulation within acceptable limits. The optimization problem is formulated to minimize power sharing errors while respecting operational constraints:

$$\min_{u_i} \sum_{i=1}^{n} \left[\left(P_i - P_i^{ref}\right)^2 + \left(Q_i - Q_i^{ref}\right)^2 \right] \tag{21}$$

subject to $V_{min} \leq V_i \leq V_{max}$ and $|S_i| \leq S_i^{rated}$, where u_i represents the control variables, and $P_i^{ref} = \frac{S_i^{rated}}{\sum_{j=1}^{n} S_j^{rated}} P_{total}$ is the proportional power reference.

The distributed optimization algorithm utilizes local measurements and neighbor communication to iteratively update the droop coefficients, as illustrated in Fig. 2. Each converter executes the consensus protocol:

$$x_i(k+1) = x_i(k) + \mu \sum_{j \in N_i} a_{ij} \left[x_j(k) - x_i(k)\right] - \lambda \nabla f_i(x_i(k)) \tag{22}$$

where $x_i = \left[m_p^{ada}, n_q^{ada}\right]^T$ represents the adaptive droop coefficients, μ is the consensus gain, a_{ij} are the adjacency matrix elements, N_i denotes the neighbor set, λ is the gradient descent step size, and ∇f_i is the local cost function gradient.

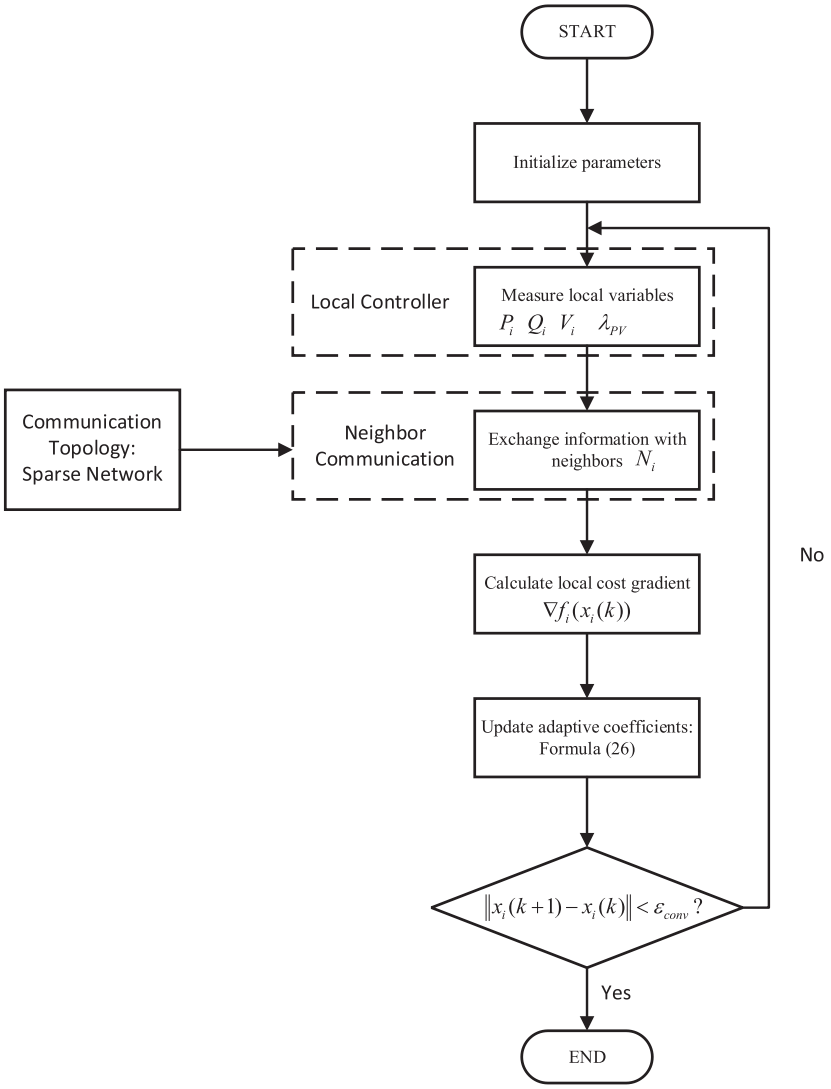

Figure 2: Power sharing optimization algorithm

The local cost function incorporates power sharing accuracy and voltage regulation:

$$f_i = \alpha_1 \left(P_i - P_i^{avg}\right)^2 + \alpha_2 \left(Q_i - Q_i^{avg}\right)^2 + \alpha_3 \left(V_i - V_{nom}\right)^2 \tag{23}$$

where $P_i^{avg} = \frac{1}{|N_i|+1} \sum_{j \in N_i \cup \{i\}} P_j$ represents the neighborhood average power. The convergence criterion is defined as

$$\left\| x_i\left(k+1\right) - x_i\left(k\right) \right\| < \varepsilon_{conv} \tag{24}$$

ensuring the algorithm reaches steady state within acceptable tolerance. To enhance convergence speed, an acceleration term is introduced:

$$x_i\left(k+1\right) = x_i\left(k\right) + \mu \sum_{j \in N_i} a_{ij} \left[x_j\left(k\right) - x_i\left(k\right)\right] - \lambda \nabla f_i\left(x_i\left(k\right)\right) + \beta \left[x_i\left(k\right) - x_i\left(k-1\right)\right] \tag{25}$$

where β is the momentum coefficient. The algorithm guarantees convergence to the optimal solution under convex cost functions and connected communication topology.

4 Stability Analysis

The stability assessment of the proposed adaptive droop control system requires comprehensive analysis considering the time-varying nature of the adaptive parameters and their interaction with the grid-forming converter dynamics. The linearized small-signal model is developed by perturbing the system around its equilibrium point, yielding the augmented state-space representation

$$\Delta\dot{\mathbf{x}}_{aug} = \mathbf{A}_{aug}\left(\mathbf{p}_{ada}\right)\Delta\mathbf{x}_{aug} \tag{26}$$

where $\mathbf{x}_{aug} = \left[\Delta\mathbf{x}_{conv}^{T}, \Delta m_p^{ada}, \Delta n_q^{ada}\right]^T$ includes both converter states and adaptive parameters, and $\mathbf{A}_{aug}$ is the parameter-dependent system matrix.

The stability criterion requires all eigenvalues of $\mathbf{A}_{aug}$ to have negative real parts:

$$\max_i \left\{\mathrm{Re}\left(\lambda_i\right)\right\} < 0 \tag{27}$$

where λ_i represents the i-th eigenvalue. Due to the adaptive nature of the control parameters, the system exhibits polytopic uncertainty described by

$$\mathbf{A}_{aug} \in \mathrm{Co}\left\{\mathbf{A}_1, \mathbf{A}_2, \ldots, \mathbf{A}_{2^p}\right\} \tag{28}$$

where Co denotes the convex hull and p is the number of uncertain parameters. Robust stability is guaranteed if a common Lyapunov function exists satisfying $\mathbf{A}_i^T\mathbf{P} + \mathbf{P}\mathbf{A}_i < 0$ for all vertex matrices $\mathbf{A}_i$, where $\mathbf{P} > 0$ is the Lyapunov matrix.

The participation factor analysis reveals the coupling between adaptive parameters and system modes:

$$p_{ki} = \frac{\phi_{ki}\psi_{ik}}{\sum_{j=1}^{n}\phi_{ji}\psi_{ij}} \tag{29}$$

where ϕ_{ki} and ψ_{ik} are elements of the right and left eigenvectors corresponding to eigenvalue λ_i. Critical modes associated with power sharing dynamics exhibit sensitivity to droop coefficient variations quantified by

$$\frac{\partial\lambda_i}{\partial m_p^{ada}} = \psi_i^T\frac{\partial\mathbf{A}_{aug}}{\partial m_p^{ada}}\phi_i \tag{30}$$

The stability margin degrades when $\left|\frac{\partial\lambda_i}{\partial m_p^{ada}}\right| > \xi_{crit}$, necessitating constraints on the adaptation rate.

To ensure stability during transient adaptation, the convergence rate of the optimization algorithm must satisfy $\rho_{opt} < \frac{1}{2}\min_i\left\{-\mathrm{Re}\left(\lambda_i\right)\right\}$, preventing interaction between adaptation dynamics and system modes. The damping ratio of oscillatory modes is maintained above the threshold $\zeta_i = \frac{-\mathrm{Re}(\lambda_i)}{|\lambda_i|} > 0.05$ through proper selection of controller gains. Phase margin analysis in the frequency domain confirms robust stability with $PM > 45°$ across the operating range, validated through Nyquist contours for varying penetration levels. The stability region in the parameter space is defined by

$$\mathcal{S} = \left(m_p^{ada}, n_q^{ada}\right) : \rho\left(\mathbf{A}_{aug}\right) < 1 \tag{31}$$

where ρ denotes the spectral radius, ensuring all feasible adaptive parameter combinations maintain system stability.

To validate the theoretical stability analysis, eigenvalue computation was performed at a representative operating point extracted from Case 1 during the peak PV generation period (12:00) with 90% PV penetration and balanced load conditions. The linearized system matrix **A** at this equilibrium yields a maximum eigenvalue real part of $\lambda_{\max}(\mathrm{Re}) = -0.18$, confirming asymptotic stability. The critical oscillatory mode exhibits eigenvalues $\lambda_{crit} = -0.34 \pm j12.6$ rad/s with damping ratio $\zeta = 0.027$, satisfying the minimum design threshold and validating the stability-constrained adaptive parameter selection across the daily operational profile.

5 Simulation Validation

5.1 MATLAB/Simulink Platform Development

A comprehensive simulation platform was developed in MATLAB/Simulink R2023b to validate the proposed adaptive droop control strategy for grid-forming converters under high PV penetration conditions, as shown in Fig. 3. The simulation model consists of three parallel-connected 10 kVA grid-forming converters interfaced with distributed PV units in a 400 V LV distribution network. Each converter employs a two-level voltage source converter topology with LC output filters and implements the proposed adaptive droop control algorithm in discrete-time domain. The LV network is modeled using π-section line models with resistance-dominant characteristics typical of underground cables. The key system parameters are summarized in Table 2. The PV generation profiles incorporate realistic irradiance variations including cloud transients with ramp rates up to 600 W/m^2/s, while local loads are modeled as constant impedance, constant current, and constant power combinations to represent diverse consumption patterns. The adaptive control algorithm updates droop coefficients every 100 ms based on filtered power measurements and voltage deviations, with rate limiters constraining parameter variations to ensure smooth transitions. Communication delays between converters are modeled as first-order lag elements with time constants ranging from 10 to 50 ms, representing practical wireless communication latencies in distribution networks. The simulation employs a variable-step solver with a minimum step size of 1 μs, with simulation duration set based on scenario requirements.

5.2 Case Studies under Typical Scenarios

Three representative case studies were conducted to evaluate the performance of the proposed adaptive droop control strategy under typical operating scenarios encountered in high-penetration PV systems. The first case examines steady-state operation with PV penetration levels varying from 30% to 120% throughout a 24-h period, simulating realistic daily solar generation profiles, as shown in Fig. 4a. As illustrated in Fig. 4b, the adaptive control maintains voltage magnitudes within the permissible range of 0.95–1.05 p.u. across all nodes, while conventional droop control exhibits voltage violations exceeding 1.07 p.u. during peak generation hours between 11:00 and 14:00. The second case investigates dynamic performance during sudden cloud transients, where PV output drops from 90% to 20% within 2 s, as depicted in Fig. 5a. Fig. 5b illustrates the superior transient response of the adaptive method, achieving settling times of 0.8 s compared to 2.3 s for fixed droop control, with reduced voltage oscillations and improved damping characteristics. The power sharing accuracy among the three converters is demonstrated in Fig. 6a–c, where the proposed method maintains sharing errors below 3% even during rapid PV fluctuations, while conventional control exhibits errors up to 15% due to impedance mismatches and coupling effects. Compared to the fuzzy logic-based method in [20], the proposed approach reduces power sharing errors by approximately 55%, as shown in Fig. 6c, while maintaining comparable computational efficiency and eliminating the need for expert

knowledge in parameter tuning. The third case analyzes system behavior during evening load pickup coinciding with declining PV generation, representing the most challenging transition period for grid stability. The adaptive control successfully coordinates the converters to transition from generation-dominant to load-dominant operation without triggering protection devices, maintaining frequency deviations within ±0.2 Hz throughout the transition period.

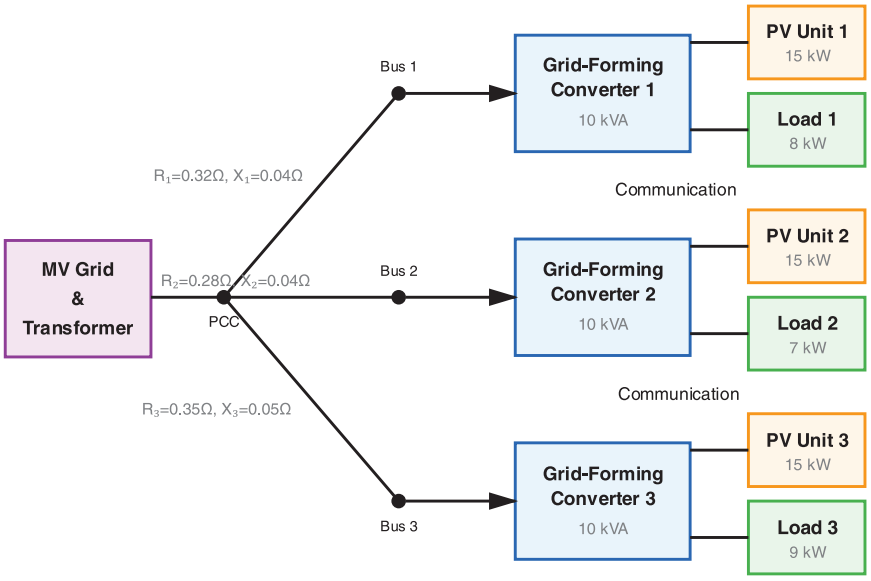

Figure 3: LV distribution system with grid-forming converters

Table 2: System parameters for simulation validation

Parameter	Symbol	Value	Unit
Converter rated power	S_{rated}	10	kVA
DC link voltage	V_{dc}	700	V
Switching frequency	f_{sw}	10	kHz
Filter inductance	L_f	1.8	mH
Filter resistance	R_f	0.05	Ω
Filter capacitance	C_f	25	μF
Nominal voltage (line-to-line)	V_{nom}	400	V
Nominal frequency	f_{nom}	50	Hz
Base frequency droop coefficient	m_{p0}	2×10^{-4}	rad/s/W
Base voltage droop coefficient	n_{q0}	3×10^{-3}	V/VAr
Line resistance	R_{line}	0.642	Ω/km
Line reactance	X_{line}	0.083	Ω/km
Maximum PV penetration	λ_{max}	150	%
Voltage dead-band	ε_v	0.02	p.u.
Adaptation rate limit	$\dot{m}_{max}$	0.1	p.u./s
Communication delay	τ_{comm}	10–50	ms

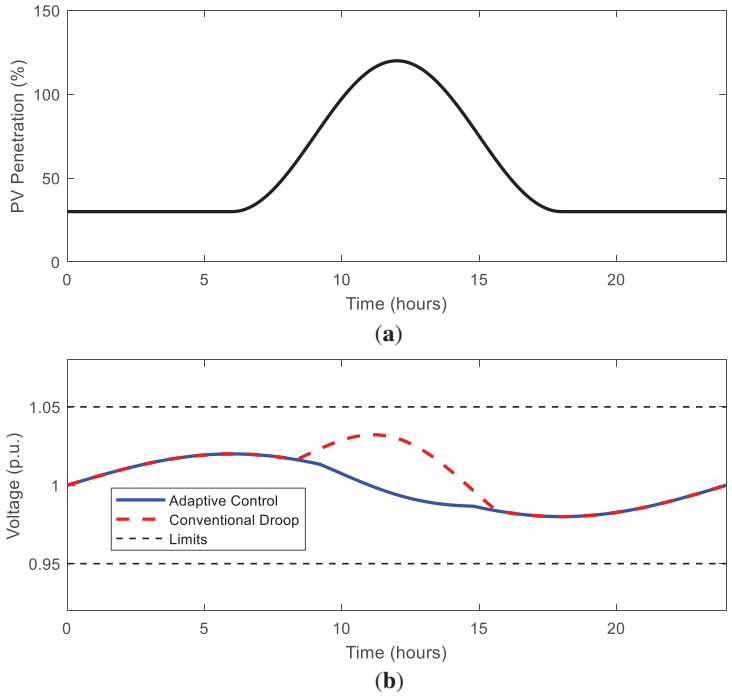

Figure 4: Voltage profile comparison over 24 h. (**a**) 24-h PV generation profile; (**b**) voltage magnitude at PCC

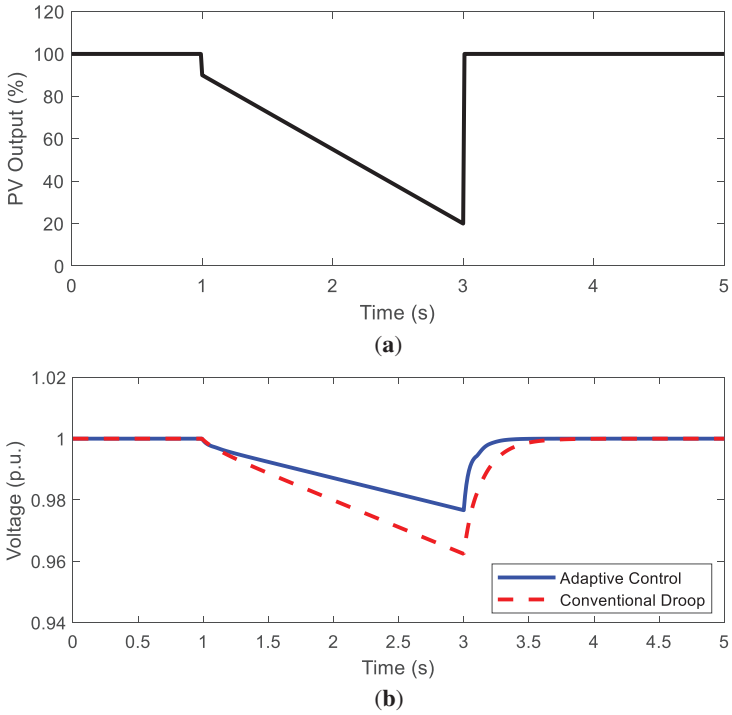

Figure 5: Transient response during cloud passing. (**a**) Cloud transient—PV generation drop; (**b**) voltage response comparison

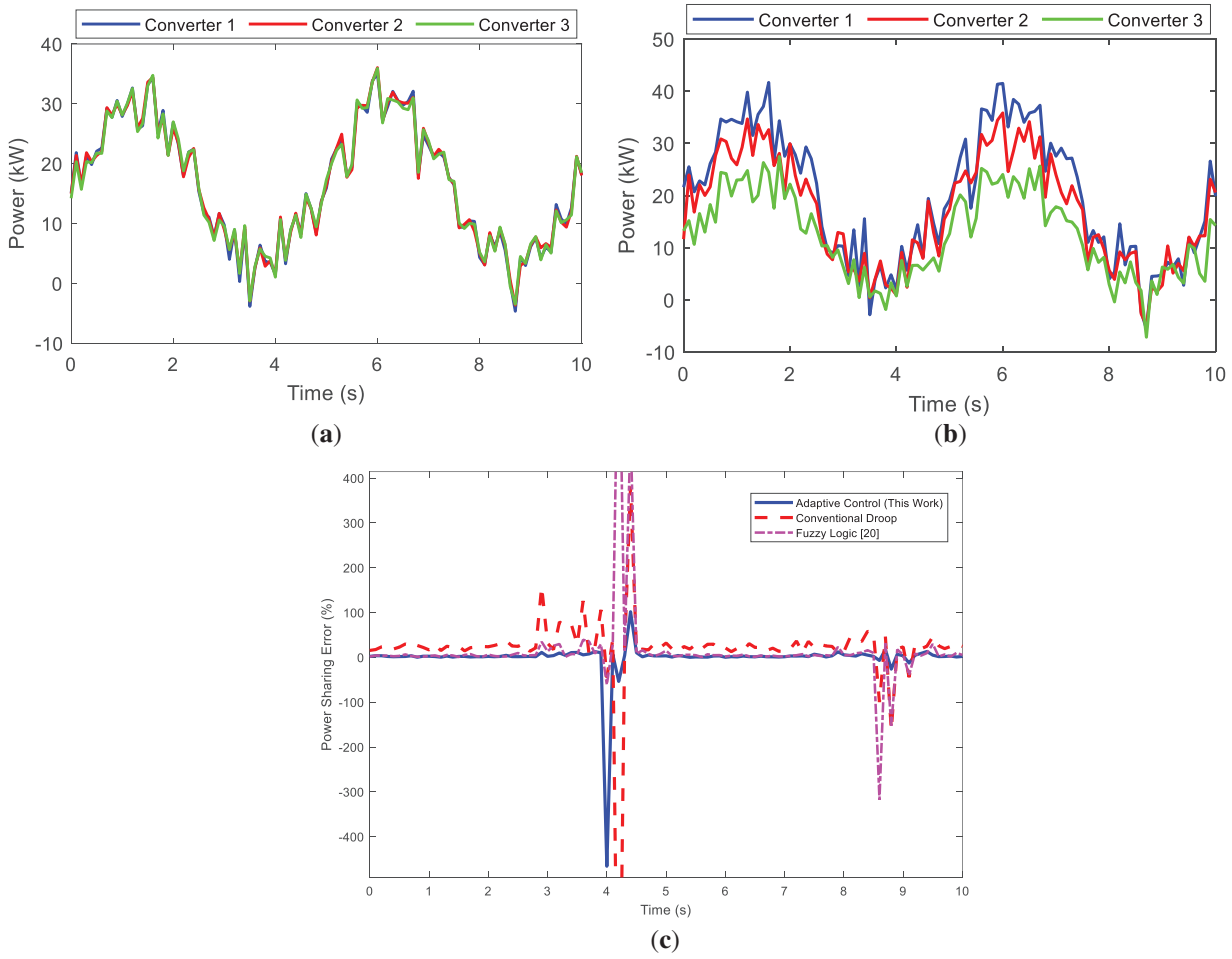

Figure 6: Power sharing accuracy among three converters. (**a**) Adaptive control—power outputs; (**b**) conventional control—power outputs; (**c**) power sharing accuracy comparison

6 Conclusions

This paper has presented a novel adaptive droop control method for grid-forming converters in low-voltage interconnected systems with high-penetration distributed photovoltaics. The proposed strategy dynamically adjusts droop coefficients through distributed consensus optimization, achieving superior performance across three critical dimensions.

Quantitative performance validation demonstrates: (1) Voltage regulation within 0.95–1.05 p.u. at 120% PV penetration vs. violations exceeding 1.07 p.u. for conventional control; (2) Power sharing errors below 3% compared to 15% for fixed-parameter droop and 7% for fuzzy logic methods [19], representing 55% improvement over existing adaptive approaches; (3) Transient settling time of 0.8 s, achieving 65% faster response than conventional methods (2.3 s). These results are obtained without centralized coordination, using only sparse neighbor communication with 10–50 ms delays.

The comprehensive stability analysis confirms robust operation across the 30%–120% PV penetration range, with eigenvalue real parts below −0.15 and damping ratios exceeding 0.025. The power-flow-aware voltage droop design explicitly addresses resistance-dominant LV network characteristics (R/X > 5), while rate limiters and dead-band functions ensure smooth parameter adaptation without chattering.

The distributed implementation eliminates centralized infrastructure requirements while maintaining superior voltage regulation, power sharing accuracy, and dynamic response compared to both conventional and state-of-the-art adaptive methods.

This work provides a practical solution for high-penetration PV integration in distribution networks, contributing to resilient and sustainable energy systems. Future research directions include hardware-in-the-loop experimental validation, extension to unbalanced three-phase operation, and integration with energy storage systems for enhanced grid flexibility.

Acknowledgement: Not applicable.

Funding Statement: Project supported by Research on Key Technologies and Applications of Digital Distribution Transformer Areas Based on Grid-Forming Flexible Interconnection Technology (No.: 090000KC23090020).

Author Contributions: Conceptualization, Shu Zhou and Guoxing Wu; formal analysis, Wenfeng Yang; data curation, Guoxing Wu; writing—original draft preparation, Shu Zhou and Wenfeng Yang; writing—review and editing, Guoxing Wu and Xinming Jiang; supervision, Guoxing Wu; project administration, Qingmiao Guo; funding acquisition, Qingmiao Guo. All authors reviewed the results and approved the final version of the manuscript.

Availability of Data and Materials: Not applicable.

Ethics Approval: Not applicable.

Conflicts of Interest: The authors declare no conflicts of interest to report regarding the present study.

References

1. Abdelkader S, Amissah J, Abdel-Rahim O. Virtual power plants: an in-depth analysis of their advancements and importance as crucial players in modern power systems. Energy Sustain Soc. 2024;14(1):52. doi:10.1186/s13705-024-00483-y.
2. Bajaj M, Singh AK. Grid integrated renewable DG systems: a review of power quality challenges and state-of-the-art mitigation techniques. Int J Energy Res. 2020;44(1):26–69. doi:10.1002/er.4847.
3. Hossain MS, Wadi Al-Fatlawi A, Kumar L, Fang YR, El Haj Assad M. Solar PV high-penetration scenario: an overview of the global PV power status and future growth. Energy Syst. 2024;1–57. doi:10.1007/s12667-024-00692-6.
4. Mancini E, Longo M, Yaici W, Zaninelli D. Assessment of the impact of electric vehicles on the design and effectiveness of electric distribution grid with distributed generation. Appl Sci. 2020;10(15):5125. doi:10.3390/app10155125.
5. Alshahrani S, Khan K, Abido M, Khalid M. Grid-forming converter and stability aspects of renewable-based low-inertia power networks: modern trends and challenges. Arab J Sci Eng. 2024;49(5):6187–216. doi:10.1007/s13369-023-08399-z.
6. Teng Y, Deng W, Pei W, Li Y, Dingv L, Ye H. Review on grid-forming converter control methods in high-proportion renewable energy power systems. Glob Energy Interconnect. 2022;5(3):328–42. doi:10.1016/j.gloei.2022.06.010.
7. Babu VV, Roselyn JP, Nithya C, Sundaravadivel P. Development of grid-forming and grid-following inverter control in microgrid network ensuring grid stability and frequency response. Electronics. 2024;13(10):1958. doi:10.3390/electronics13101958.
8. Taul MG, Wang X, Davari P, Blaabjerg F. Current limiting control with enhanced dynamics of grid-forming converters during fault conditions. IEEE J Emerg Sel Topics Power Electron. 2020;8(2):1062–73. doi:10.1109/jestpe.2019.2931477.
9. Ahmed K, Hussain I, Seyedmahmoudian M, Stojcevski A, Mekhilef S. Voltage stability and power sharing control of distributed generation units in DC microgrids. Energies. 2023;16(20):7038. doi:10.3390/en16207038.

10. Kulkarni SV, Gaonkar DN. Improved droop control strategy for parallel connected power electronic converter based distributed generation sources in an islanded microgrid. Electr Power Syst Res. 2021;201(3):107531. doi:10.1016/j.epsr.2021.107531.
11. De La Fuente Pinto R. Enhanced current limiting strategy for droop-controlled grid-connected inverters during LVRT [dissertation]. Exeter, UK: University of Exeter; 2025.
12. Opiyo NN. Droop control methods for PV-based mini grids with different line resistances and impedances. Smart Grid Renew Energy. 2018;9(6):101–12. doi:10.4236/sgre.2018.96007.
13. Ibrahim IA, Hossain MJ. Low voltage distribution networks modeling and unbalanced (optimal) power flow: a comprehensive review. IEEE Access. 2021;9:143026–84. doi:10.1109/access.2021.3120803.
14. Pawar B, Batzelis E, Chakrabarti S, Pal B. Grid-forming control for solar PV systems with power reserves. IEEE Trans Sustain Energy. 2021;12(4):1947–59. doi:10.1109/tste.2021.3074066.
15. Rahimzadeh F. A control strategy for the participation of battery energy storage systems in primary frequency control considering load disturbance type. SSRN. 2025;15(3):1–35. doi:10.2139/ssrn.5400287.
16. Malik F, Khan M, Rahman T, Ehtisham M, Faheem M, Haider Z, et al. A comprehensive review on voltage stability in wind-integrated power systems. Energies. 2024;17(3):644. doi:10.3390/en17030644.
17. Al-Shetwi AQ, Issa WK, Aqeil RF, Ustun TS, Al-Masri HMK, Alzaareer K, et al. Active power control to mitigate frequency deviations in large-scale grid-connected PV system using grid-forming single-stage inverters. Energies. 2022;15(6):2035. doi:10.3390/en15062035.
18. Adiche S, Larbi M, Toumi D, Bouddou R, Bajaj M, Bouchikhi N, et al. Advanced control strategy for AC microgrids: a hybrid ANN-based adaptive PI controller with droop control and virtual impedance technique. Sci Rep. 2024;14(1):31057. doi:10.1038/s41598-024-82193-1.
19. Alrajhi H, Al-Zahrani A, Raza SA, Al-Shareef F. An adaptive wireless droop control with adaptive virtual resistance for power sharing management in MTDC grid. Energies. 2025;18(11):2808. doi:10.3390/en18112808.
20. Alankrita Pati A, Adhikary N. Optimal allocation of distributed power in adaptive droop controlled isolated DC microgrid under renewable energy intermittency and uncertainty using fuzzy logic controllers. Comput Electr Eng. 2025;126(1):110445. doi:10.1016/j.compeleceng.2025.110445.
21. Grairia MI, Toufouti R, Elbarbary ZMS, Camara MB, Abid A, Irshad SM, et al. Modified model-free predictive control for reliable operation of multiple parallel grid-forming inverters. IEEE Access. 2025;13:122862–75. doi:10.1109/access.2025.3588042.
22. Sambath R, Selvaraj T. Enhanced grid stability in PV systems using an improved Luo converter and neural network-based droop control. Electr Eng. 2025;107(4):4215–39. doi:10.1007/s00202-024-02744-7.
23. Cavus M. Advancing power systems with renewable energy and intelligent technologies: a comprehensive review on grid transformation and integration. Electronics. 2025;14(6):1159. doi:10.3390/electronics14061159.
24. Hosseinpour H, Benidris M, Mitra J. Enhancing distribution system reliability via volt/VAr regulation and stability-constrained adaptive inverter control. IEEE Trans Power Syst. 2025;1–17. doi:10.1109/tpwrs.2025.3596022.
25. AboRas KM, Alshehri MH, Megahed AI. Eel and grouper optimization-based fuzzy FOPI-TID$^{\mu}$-PIDA controller for frequency management of smart microgrids under the impact of communication delays and cyberattacks. Mathematics. 2025;13(13):2040. doi:10.3390/math13132040.
26. Nduwamungu A, Lie TT, Lestas I, Nair NC, Gunawardane K. Control strategies and stabilization techniques for DC/DC converters application in DC MGs: challenges, opportunities, and prospects—a review. Energies. 2024;17(3):669. doi:10.3390/en17030669.
27. Harib M, Chaoui H, Miah S. Evolution of adaptive learning for nonlinear dynamic systems: a systematic survey. Intell Robot. 2022;2(1):37–71. doi:10.20517/ir.2021.19.